EJN European Journal of Neuroscience

FENS Federation of European Neuroscience Societies

European Journal of Neuroscience, Vol. 40, pp. 3774–3784, 2014 doi:10.1111/ejn.12749

COGNITIVE NEUROSCIENCE

Spectrotemporal dynamics of the EEG during working memory encoding and maintenance predicts individual behavioral capacity

Pouya Bashivan,[1] Gavin M. Bidelman[2,3] and Mohammed Yeasin[1,2]
[1]Department of Electrical and Computer Engineering, University of Memphis, Memphis, 38152 TN, USA
[2]Institute for Intelligent Systems, University of Memphis, Memphis, TN, USA
[3]School of Communication Sciences & Disorders, University of Memphis, Memphis, TN, USA

Keywords: alpha power, independent component analysis (ICA), induced brain responses, memory load, neural oscillation, visual working memory

Abstract

We investigated the effect of memory load on encoding and maintenance of information in working memory. Electroencephalography (EEG) signals were recorded while participants performed a modified Sternberg visual memory task. Independent component analysis (ICA) was used to factorise the EEG signals into distinct temporal activations to perform spectrotemporal analysis and localisation of source activities. We found 'encoding' and 'maintenance' operations were correlated with negative and positive changes in α-band power, respectively. Transient activities were observed during encoding of information in the bilateral cuneus, precuneus, inferior parietal gyrus and fusiform gyrus, and a sustained activity in the inferior frontal gyrus. Strong correlations were also observed between changes in α-power and behavioral performance during both encoding and maintenance. Furthermore, it was also found that individuals with higher working memory capacity experienced stronger neural oscillatory responses during the encoding of visual objects into working memory. Our results suggest an interplay between two distinct neural pathways and different spatiotemporal operations during the encoding and maintenance of information which predict individual differences in working memory capacity observed at the behavioral level.

Introduction

A fundamental building block of human cognition is working memory (WM), that is, the amount of information temporally held and manipulated in the mind. Understanding the effect of cognitive load on WM and examining its neurophysiological underpinnings has been the motivation for numerous studies (Cohen *et al.*, 1997; Luck & Vogel, 1997). Baddeley's model (Baddeley, 2000) remains a common explanation for information processing in the brain. According to this model, verbal and non-verbal information are stored within different sub-systems of WM. However, overlapping brain activations have been found between the two within large areas; this suggests that they are operated upon by common mechanism (e.g., a 'memory buffer'; Salo *et al.*, 2013). While methodology and domain of investigation vary across studies, previous work generally agrees that five to seven items can be adequately stored and manipulated in WM (Cowan, 2005).

Neurophysiological correlates of WM have been studied using various brain imaging techniques including functional magnetic resonance imaging (fMRI), electroencephalography (EEG) and magnetoencephalography (MEG). Using event-related brain potentials (ERPs), Vogel & Machizawa (2004) reported that a sustained component of the ERP (contralateral delay activity) was saturated at around four items in a visual WM task. Moreover, strong correlations were found between individual WM capacity and the sustained neural activity generated during the maintenance of information. Similar correlations have been reported during memory maintenance of non-musical tones (Lefebvre *et al.*, 2013; Grimault *et al.*, 2014) and numbers (Golob & Starr, 2004) using the same neural signature. While ERP responses capture the time-locked activity of the brain, they fail to detect neural responses that are not directly phase-locked to the stimulus presentation (i.e., induced brain activity).

Event-related synchronisation and desynchronisation were introduced to capture such non-phase-locked induced responses by observing power changes in the EEG during perceptual and cognitive processes (Pfurtscheller & Lopes, 1999). The most consistent effect reported in the literature has been the increase in α-band (8–13 Hz) power with higher memory loads during WM maintenance (Jensen *et al.*, 2002; Tuladhar *et al.*, 2007). In contrast, in a recent study, Okuhata *et al.* (2013) reported positive and negative changes in α-power in parietal cortex with successive vs. simultaneous versions of a Sternberg task, respectively. Examining human intracranial EEG recordings, Meltzer *et al.* (2008) illustrated that the increase and decrease in α- and θ-band (4–7 Hz) power during WM

Correspondence: Pouya Bashivan, [1]Computer Vision, Perception and Image Analysis (CVPIA) Lab, as above.
E-mail: pbshivan@memphis.edu

Received 2 June 2014, revised 8 September 2014, accepted 9 September 2014

were strictly localised to frontal and parietal midline locations. These findings suggest that frequency-specific power changes are not a unitary phenomenon but rather depend on cortical location, time and the nature of a given cognitive WM task.

A number of studies have also examined the effect of memory load on neural activity as inferred from blood oxygen level-dependent (BOLD) signals recorded via fMRI. Cohen *et al.* (1997) illustrated differences in activation in frontal, parietal and occipital areas in response to different memory loads in an *n*-back task. Furthermore, two other studies also found similarly distributed areas associated with WM during Sternberg (Kirschen *et al.*, 2010) and visual WM (Todd & Marois, 2004) tasks. Recently, direct multimodal comparisons have shown that fMRI BOLD signals are negatively correlated with α-band modulation, as recorded via EEG and MEG (Meltzer *et al.*, 2007). This suggests a fundamental link between divergent neuroimaging methodologies, namely, that negative BOLD responses are associated with cognitive WM activity analogous to the oscillatory α modulations recorded via the EEG.

In the current study, we investigated the effects of memory load on spectrotemporal properties of brain waves as observed from the scalp-recorded EEG. The current paradigm allows us to extend recent ERP studies (Vogel & Machizawa, 2004; Lefebvre *et al.*, 2013) by characterising the induced oscillatory brain activity generated during WM operations using a noninvasive methodology (Meltzer *et al.*, 2008). Additionally, while the encoding stage is often neglected in the studies related to memory load (Jensen *et al.*, 2002; Meltzer *et al.*, 2007), we studied the responses during encoding and maintenance of information to uncover how neurophysiological processing across the timespan of WM relates to an individual's behavioral capacity limits. We anticipated that induced neural oscillations in parietal and frontal cortices would systematically change with memory load. Furthermore, we expected that these neural markers representing the number of items maintained in WM should not increase for set sizes above an individual's behavioral capacity limit.

Materials and methods

Participants

Fifteen graduate students (eight female) participated in the study. Participants were between 24 and 33 years of age ($\mu \pm \sigma$: 28 ± 3 years) and all but one were strongly right-handed as measured by the Edinburgh Handedness Inventory (laterality index > 95%) (Oldfield, 1971). Data from two of the subjects were excluded from further analyses because of frequent myogenic artifacts in their EEGs. All participants had normal or corrected-to-normal vision. Subjects reported no history of visual or neuropsychiatric disorders, nor were currently on medication. The experiment was undertaken with the understanding and written informed consent of each participant, in compliance with the Declaration of Helsinki and a protocol approved by the University of Memphis Institutional Review Board. Participants were compensated for their time.

Stimuli and task

We adopted a modified version of the Sternberg memory task (Sternberg, 1966). This task is suitable for studying WM because it can systematically be configured for different memory loads. It also temporally separates encoding, maintenance, and recall stages of the WM process. On each trial, subjects briefly (500 ms) observed a matrix consisting of different English characters positioned around a center point ('SET'; Fig. 1). Characters were displayed with white color over a black background. The size of each character was 1.15°; they were distributed around a center fixation cross and within a visual angle of 2.9°. Array size varied randomly on each trial (two, four, six or eight items). In all variations of the task, characters were displayed in an array such that their distribution on the left and right side of the center point was the same. After a 3-s delay (i.e., maintenance stage), a 'TEST' character was shown on the center of the screen. Subjects responded via a button press to indicate whether this character had occurred in the previous memory SET.

On half the trials, the test item occurred in the SET on the other half it did not. Subjects were encouraged to respond as accurately as possible, and feedback was given via a colored light on the screen, 300 ms after the participant's response. The next trial was initiated after a 3.4-s inter-stimulus interval. Following 20 practice trials for task familiarisation, subjects completed 60 experimental trials per set-size condition. The number of correct and incorrect responses for each set size were then used to compute the WM capacity for each participant (i.e., the number of items successfully held in memory). WM capacity was also calculated for each set size and participant using the WM capacity index, K, defined as $K = S(H\text{-}F)$, where S is the number of items in the memory array, H is the hit rate and F is the false alarm rate (Pashler, 1988; Cowan, 2000).

Subjects were seated inside an electroacoustically shielded booth. They were instructed to avoid body movement and restrict their visual gaze during the task by fixating on the center of the screen. The visual WM task was presented on an LCD monitor at a distance of 1 m. Periodic breaks (~ 5 min) were given between experimental blocks, which lasted ~ 15–16 min depending on response speed. The visual stimuli were implemented in MATLAB using the Psychophysics Toolbox (Brainard, 1997). In addition to accuracy, response times (RTs) were also recorded during the experiment, computed as the time-lapse between the appearance of the TEST character and the participant's response.

EEG recording and analysis

Neuroelectric responses were recorded using standard procedures reported by our laboratory (Bidelman *et al.*, 2013, 2014) Briefly, the continuous EEG was recorded from 64 sintered Ag/AgCl electrodes placed around the scalp at standard 10-10 locations (Oostenveld & Praamstra, 2001) (Neuroscan, Quik-cap). Electrodes placed on the outer canthi of the eyes and the superior and inferior orbit were used to monitor ocular activity. Data were digitised with a sampling rate of 500 Hz using an online filter passband from DC to 250 Hz. Electrode impedance was maintained ≤ 5 kΩ over the duration of the experiment. During online acquisition, neural responses were referenced to an electrode placed ~ 1 cm posterior to Cz. However, data were re-referenced off-line to a common average reference for subsequent analyses.

For the analysis, EEG data were down-sampled to 250 Hz, and baseline-corrected by removing the average of each channel. Ocular artifacts (saccades and blink artifacts) were corrected in the EEG using principal component analysis (Wallstrom *et al.*, 2004). Responses were then bandpass-filtered from 1 to 45 Hz using a zero-phase (two-pass) FIR filter of order 500 for visualisation and response quantification (EEGLAB function pop_eegfiltnew). For each set size condition, EEG data was segmented into periods of 9000 ms starting from 2000 ms before presentation of SET to 3500 ms after presentation of TEST. Independent component analysis (ICA; see below for details) was then applied on the concatenated

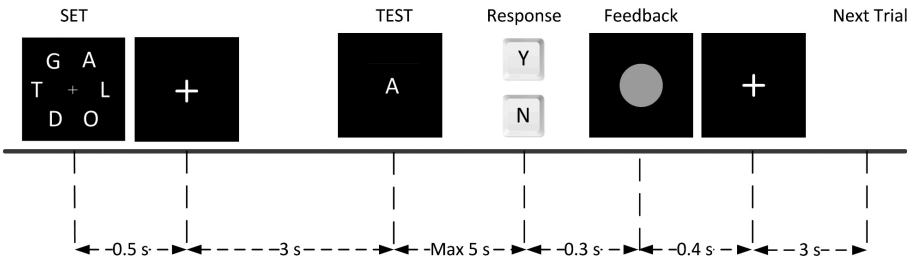

FIG. 1. Time course of the modified Sternberg visual WM task paradigm. Shown here are the sequence of stimulus events as displayed on the computer screen. Each trial started by appearance of an array of characters (SET) around a center point for a brief period (500 ms). SET was then replaced by a cross in the middle of the screen for 3000 ms during which participants were asked to subvocally rehearse the characters. Next, a test character was shown in the middle of the screen (TEST) and the participant responded by pressing one of the two buttons to indicate whether TEST was among SET or not. A green or red circle was presented on the screen to indicate correct or incorrect response. A 3000 ms inter-trial interval was then followed with a cross in the middle of the screen. Set size was chosen randomly for each trial.

set of multi-channel epoched trials, including all subjects and conditions, decomposing the recorded signals into statistically independent source signals (Makeig *et al.*, 1996). The number of independent sources equaled the number of channels.

Event-related spectral perturbation (ERSP) of each ICA signal was computed to study the time–frequency changes in the EEG across memory loads (Makeig, 1993). Only correct response trials were considered in the analysis. For the current study, the ERSP is desirable as it also captures non-phase-locked neural activity, induced by the stimulus presentation, that is not observable with traditional evoked potential averaging (Schomer & Da Silva, 2012). ERSPs were computed by calculating the mean change in spectral power (in dB) from baseline for different frequency and latencies using a complex Morlet wavelet transform (Tallon-Baudry *et al.*, 1997; Herrmann *et al.*, 1999). The number of cycles was selected according to the frequency (scale) and was increased from 0.5 to 13.8 for a frequency range of 1–30 Hz. It has been suggested that this approach provides better frequency resolution at higher frequencies than a conventional wavelet approach that uses constant cycle length (Delorme & Makeig, 2004). Based on these observations, we used 40 ms/0.5 Hz as the time–frequency spacing for the daughter wavelets. The baseline power spectrum was calculated for a 2-s reference period before the stimulus presentation. In order to compute the baseline power, the 2-s baseline period for all trials was extracted and the same wavelet transform as the one used for the whole trial analysis was applied on the dataset. Power values were then averaged over trials and time samples to derive the baseline power spectral density. This procedure minimised the probable effect of including post-stimulus EEG into baseline power computation (Zoefel & Heil, 2013).

The EEGLAB toolbox was used to compute the ERSP response (Makeig *et al.*, 2004). We quantified spectral perturbations as the mean power change within each frequency band of interest. Alpha (α; 8–13 Hz) and beta (β; 13–30 Hz) frequency band powers were measured for each individual from the ERSP. Significant deviations in wavelet power from the baseline were assessed using bootstrap resampling. For each trial, baseline spectral estimates were calculated from randomly selected latency windows in the specified epoch baseline and were then averaged. This process was repeated 200 times to produce a surrogate 'baseline' spectral distribution whose specified percentiles were then taken as the statistical power (Delorme & Makeig, 2004). Due to the high number of comparisons needed to generate the ERSP response for each component and condition (200 time periods $\times$ 60 frequencies), the resulting P-values were corrected using false discovery rate (FDR) with $P < 0.05$ (Benjamini & Yekutieli, 2001). In contrast to the familywise error rate (FWER) correction (e.g. Bonferroni correction) which controls the probability of single errors in rejection of null hypotheses, FDR works by controlling the proportion of the rejected null hypotheses and is therefore less conservative than FWER.

ICA

Neuroelectric signals recorded at each scalp electrode are formed by the summation of different overlapping potentials originating from various brain sources. ICA performs linear spatial filtering on the EEG data to isolate independent neuronal sources contributing to the neurophysiological signal recorded at the scalp. In addition, ICA was used to factorise the data into temporally independent components and to create dipolar scalp maps without including any geometrical information about the head or electrode placements. ICA provides a powerful means of isolating brain signals that index physiologically distinct processes (Vigário *et al.*, 2000; Jung *et al.*, 2001; Tang *et al.*, 2002; Makeig *et al.*, 2004; Lenartowicz *et al.*, 2014). Application of ICA to EEG data is under the assumption that EEG dynamics can be modeled as a collection of a number of statistically independent brain processes (Makeig *et al.*, 1996). However, transient interactions may exist between different areas of the brain during execution of cognitive tasks and, hence, this assumption is sometimes violated. In such cases, the ICA decomposes the signals into a set of maximally independent components by maximising their mutual independence (Vigário *et al.*, 2000). The derived components are temporally independent in a global sense, across the entire time course of the trial for all subjects and conditions. However, it should be noted that short-lived dependencies between components may still be present (Vakorin *et al.*, 2010), especially in a transformed domain (e.g. frequency domain). In the current study, ICA allowed us to identify maximally distinct brain sources (in a mathematical sense) that contribute to WM processing and that have otherwise been blurred in traditional ERP studies (Vogel & Machizawa, 2004).

Group-wise ICA decomposition (Vakorin *et al.*, 2010) was used in this study. ICA was applied to the data set consisting of the correct trials from all four conditions and 13 participants. Independent components were found using the extended infomax algorithm (Lee *et al.*, 1999). Projection vectors corresponding to each independent component (IC) were then extracted from the mixing matrix (W^{-1}) and were used to localise an equivalent dipole (Oostendorp & Van Oosterom, 1989). Electrode positions were registered to the MNI (Montreal Neurological Institute) brain and two symmetrical dipoles were fitted to each component using the boundary element head model (Delorme & Makeig, 2004) (v12.0.2.5b). The best-fitting

result was then selected for each IC. Selection of ICs for subsequent analysis was guided by three criteria, namely, we only considered components (i) that were non-artifactual (determined based on IC scalp topography and spectral density); (ii) whose source foci were located inside the head boundary and cerebral cortex; (iii) whose source dipoles were clearly bilateral (ICs whose dipoles were localised within ~ 10 mm were discarded). Specifically, model accuracy was measured by assessing the residual variance (RV) of the scalp map of the best-fitting dipole. Additionally, ICs with RV > 10% were discarded. While anatomical locations of each source were modeled as two point sources, only a single time course was extracted and further analysed from each IC. Source dipole localisation was computed using the DIPFIT plugin in EEGLAB performed on the ICA weighting matrix.

Summary of statistical analysis approach

ERSP responses were generated for each component (seven ICs) and condition (four set sizes). Within each ERSP response, bootstrap resampling and FDR correction (Benjamini & Yekutieli, 2001) were used to mask the insignificant time–frequency (200 × 60) points. Activity patterns were identified within different frequency bands, stages and components from these ERSPs. In order to test whether our selected features (encoding, maintenance, and alpha and beta power) were significantly changing across conditions, we conducted a one-way repeated-measures (rm)ANOVA within each IC with set size as the single factor (four levels). The rmANOVA tests were only conducted on the stage (encoding or maintenance), frequency bands (alpha or beta) and ICs which showed a consistent ERSP across all set-sizes (based on visual inspection of the time–frequency maps). Finally, we investigated the correlation between the power features and WM capacity (*K*). For each dependent measure, FDR corrected correlation analysis was performed for the number of ICs which previously showed significant change across set size (i.e., based on the initial ANOVA). For instance, in the case of alpha-average encoding power change (AEPC), ANOVA tests showed significance for four components: precuneus, fusiform gyrus (FG), cuneus and inferior parietal lobule (IPL). Therefore the correlation analysis and the follow-up FDR correction were performed within this set of ICs.

Results

Behavioral data

Mean behavioral accuracy and RTs per stimulus set size are shown in Fig. 2. Due to non-normality of RT distributions, we used each subject's median RT per set size. Significant differences in accuracy and RT across set sizes were investigated using Tukey-adjusted one-way rmANOVA. Analysis revealed differences in response accuracy across conditions ($F_{3,42} = 78.13$, $P < 0.0001$). Accuracy was high for small set size conditions (two or four items) but degraded precipitously with increasing set size (more than four items). A significant effect across memory load conditions was also found for RT ($F_{3,42} = 5.11$, $P < 0.005$). Figure 2 shows the differential in response time between adjacent set sizes. Mean slope of RT vs. set size, reflecting 'behavioral throughput' (Bidelman *et al.*, 2014), was 33 ms per item for set size 4 but decreased to ~ 10 ms per item for higher set sizes.

Mean WM capacity, as measured by *K*, is shown as a function of set size in Fig. 3. *K* values showed significant changes across set sizes ($F_{3,42} = 9.96$, $P < 0.0001$). WM capacity increased from set size 2–4 and remained constant thereafter (i.e., set sizes 4, 6 and 8). To devise a single measure of individual WM capacity, each participant's maximum *K* value across all four set sizes were calculated.

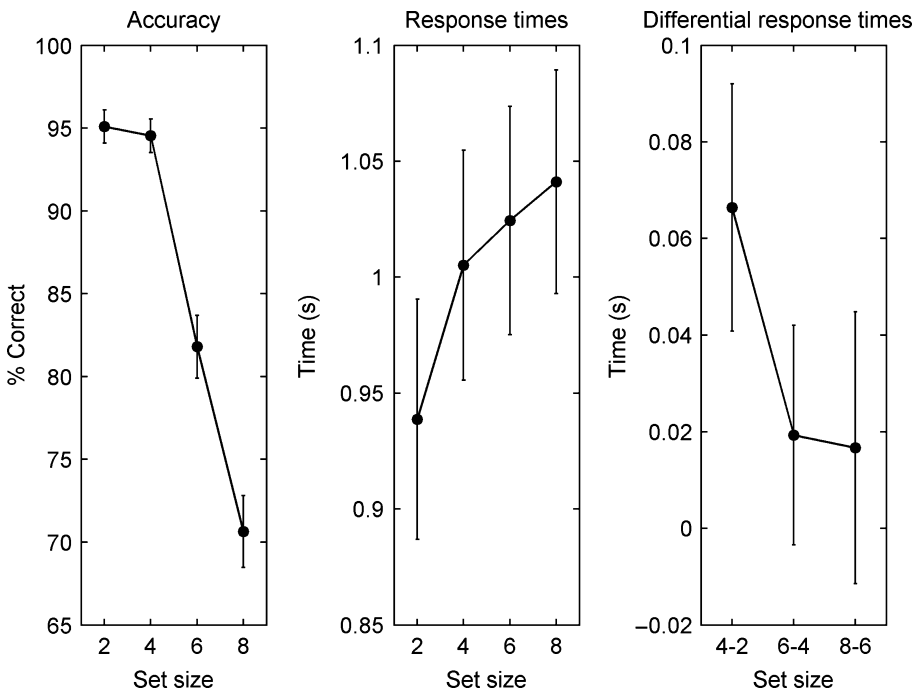

FIG. 2. Behavioral performance in visual WM. (left) Response accuracy across set sizes. Accuracy of responses degraded precipitously for set sizes > 4; (middle) response times (RTs) across set sizes; (right) difference in RTs across conditions. Slope of RT vs. set size was 33 ms per item for set size 4 and 10 ms per item for higher set sizes. Error bars are ± SEM.

Mean K across our cohort was 3.89 (0.9), indicating that about four items (on average) can be adequately maintained in WM (Vogel & Machizawa, 2004). Moreover, the variance of K increased for higher set sizes (Bartlett test on K values from four set sizes; $P < 0.0001$). Increased inter-subject variability with increasing task complexity probably reflects larger differences in the number of stored items across individuals when the set size exceeds the mean WM capacity.

Independent components of EEG

Figure 4 shows significant dipoles (RV < 10%) describing the IC component activity at the scalp. Only seven of the total 64 ICs survived our stringent selection criteria (see Materials and Methods). Component characteristics are detailed in Table 1. Corresponding source dipole locations covered brain areas including bilateral superior and inferior parietal lobule, superior temporal gyrus, postcentral gyrus, inferior frontal gyrus (IFG), FG and cuneus. ICs are sorted in descending order of mean projected variance. Essentially, ICs with lower indices have more significant loadings (i.e., they describe a higher proportion of the scalp data) compared to ICs with larger indices.

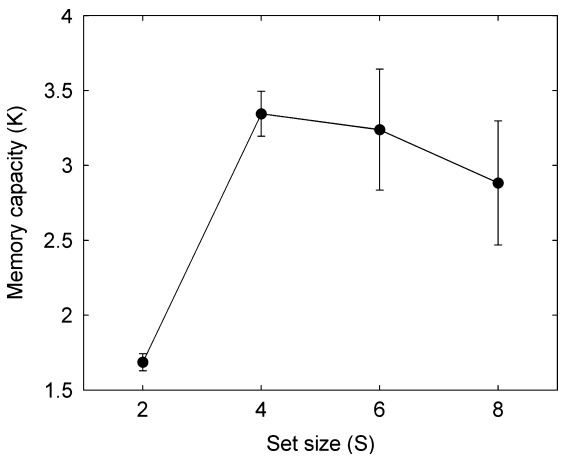

FIG. 3. Changes in working memory capacity with memory set size. Number of items stored in the memory (K) is plotted as a function of set size. K is defined as $K = S(H\text{-}F)$, where S is the number of items in the memory array, H is the hit rate and F is the false alarm rate. Working memory capacity increases at small set sizes and then plateaus thereafter, indicating a saturation of cognitive load. Error bars are ± SEM.

Examining ERSP responses within each of these ICs revealed regular patterns of activity during the encoding and maintenance stages. Figure 5 shows select ERSP spectrograms of IC2, 3 and 5, respectively. The dominant activity in the frequency domain was centered around the α-band (10 Hz) and also extended to higher frequencies in the β-band (13–30 Hz).

ERSPs extracted from FG, IPL, cuneus and precuneus showed a strong decrease in α-power starting ~ 250 ms after the presentation of the SET array that persisted ~ 2 s after the disappearance of the stimulus. Power decrease in precuneus typically unfolded over a shorter time-window than in the FG (precuneus, 1500 ms; FG, > 2000 ms). In contrast, α-power in precuneus showed a similar decrease followed by a subsequent increase in α-power not observed in the more posterior parietal sources (Fig. 5; see hot colored regions; ~ 2500 ms). In further contrast, activity in IFG consisted of a transient increase in β-power lasting through the encoding period and a continuous increase in α-power that initiated at the disappearance of the stimulus array and persisted throughout the entirety of the encoding and maintenance stages.

In order to objectively divide the response into encoding and maintenance processing stages, we examined the time course of perturbations extracted from the ERSP maps within select frequency bands. Fig. 6 shows the α-band perturbation curve extracted from the precuneus, IFG, FG and cuneus. Conforming to the ERSP response in Fig. 5, a strong decrease in the α-band power was observed within the time window following the disappearance of the stimulus set.

In order to perform numerical comparisons between oscillatory responses, two indices were computed from each ERSP within the various frequency bands: (i) AEPC, measured as the mean dB perturbation in power during a 1000-ms time window, starting from disappearance of the stimulus (t = 500 ms) until 1 s later (t = 1500 ms; see Fig. 6); (ii) average maintenance power change (AMPC), measured as the mean perturbation in power in dB units within a 1000-ms time window, starting 1 s before presentation of the test character (t = 2500 ms) and extending to its presentation (t = 3500 ms; see Fig. 6).

Encoding perturbation

α-Band AEPC became more negative with increasing set size (Fig. 7A). This effect was observed mainly in occipital (cuneus), parietal (IPL and precuneus) and temporal (FG) cortices. α-AEPC decreased linearly with increasing set size from 2 to 6 and remained almost constant thereafter. These observations were confirmed with RMANOVAS, which indicated that on average spectral power reduced monotonically with increasing memory load in all four brain areas

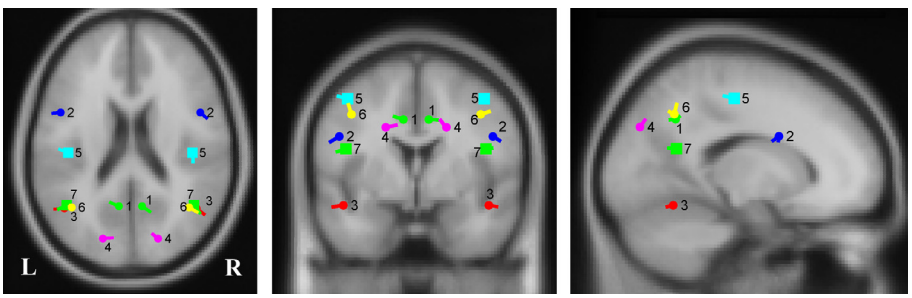

FIG. 4. Dipole locations of independent component source activations during visual WM. Fitted dipoles covered bilateral superior and inferior parietal lobule, superior temporal gyrus, postcentral gyrus, IFG, cingulate gyrus, FG and cuneus. Dipoles reflect the mean center of gravity of source component activity whose residual variance is < 10% in explaining the scalp activity. ICs which did not show significant modulations with increasing set size are illustrated with squares.

(linear contrasts: precuneus, $F_{1,36} = 34.20$, $P < 0.0001$; FG, $F_{1,36} = 14.66$, $P < 0.001$; cuneus, $F_{1,36} = 20.84$, $P < 0.0001$; IPL, $F_{1,36} = 20.05$, $P < 0.0001$). However, *post hoc* Tukey–Kramer adjusted multiple comparisons showed no significant difference between set sizes 6 and 8 (precuneus, $P = 0.99$; FG, $P = 0.98$; cuneus, $P = 1.00$; IPL, $P = 0.94$), indicating a saturation in the response at higher memory loads. As with α-power, β-AEPC in precuneus similarly decreased across set size conditions ($F_{3,36} = 8.06$, $P < 0.001$; Fig. 7B).

TABLE 1. Coordinates of the seven independent components with residual variance < 10%

IC no.	Talairach coord. (*x*,*y*,*z*)	Location	Closest BA	RV (%)
1	–8/8, –55, 37	Precuneus	7	4.74
2	–47/47, 7, 24	Inferior frontal gyrus	9	5.43
3	–45/45, –59, –11	Fusiform gyrus	37	3.42
4	–19/19, –77, 34	Cuneus	7	2.40
5	–42/42, –19, 47	Postcentral gyrus	3	1.82
6	–40/40, –56, 40	Inferior parietal lobule	40	8.75
7	–43/43, –55, 20	Superior temporal gyrus	39	4.18

BA, Brodmann area. ICs with lower numbers account for higher percentages of variance in EEG. Location column shows the closest cortical area to the dipole (www.talairach.org).

Maintenance perturbation

Figure 7C shows the change in average α-activity during the maintenance period (α-AMPC) across set size condition. Maintenance stage activity was modulated by stimulus load in precuneus ($F_{3,36} = 3.40$, $P = 0.03$) and IFG ($F_{3,36} = 3.69$, $P = 0.02$; Fig. 7C). Paralleling the behavioral pattern (e.g., Fig. 3), *post hoc* Tukey–Kramer adjusted multiple comparisons revealed that α-AMPC in IFG increased from set size 2 to 4 and saturated thereafter ($P = 0.003$). Finally, β-band synchronisation that was visible from the ERSP response of IFG did not reach significance ($F_{3,36} = 2.24$, $P = 0.1$).

Brain–behavior relations between individual WM capacity and spectrotemporal features of the EEG

We assessed the correspondence between regional activation (neural activity in precuneus, IPL, IFG, FG and cuneus, i.e. α-AEPC, α-AMPC and β-AEPC) and participants' individual behavioral WM capacity (*K*) using Pearson's correlations (Fig. 8). Only ICs showing

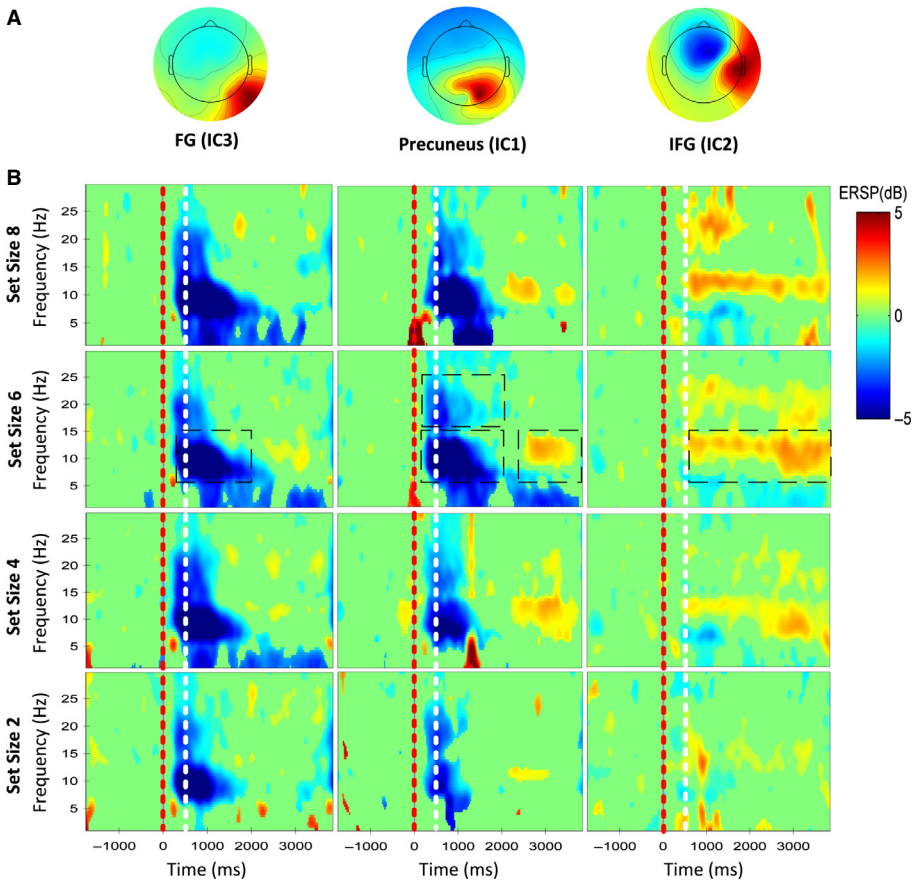

FIG. 5. Event-related spectral perturbations (ERSPs) of select independent component (IC). (A) Topography for each of the select IC components. The topographic maps reflect the spatial distribution of the group ICA component signal. (B) ERSP for select IC sources as a function of stimulus set size. Hot colors, increase in spectral power; cool colors, decrease in spectral power from baseline. Time–frequency points with nonsignificant change from baseline are masked in green at the $P < 0.05$ level (bootstrap resampling). The vertical red and white lines mark the beginning and end of the presentation of SET respectively (see Fig. 1). The source in FG was active during the encoding period with a significant decrease in α-power but no change during maintenance. In contrast, IFG showed a continuous enhancement in α-power throughout the encoding and maintenance periods and precuneus showing significant decrease in α- and β-power during the encoding and also increased α-power during the maintenance. Dashed black boxes indicate the frequency bands extracted and analysed within each component (cf. Fig. 6).

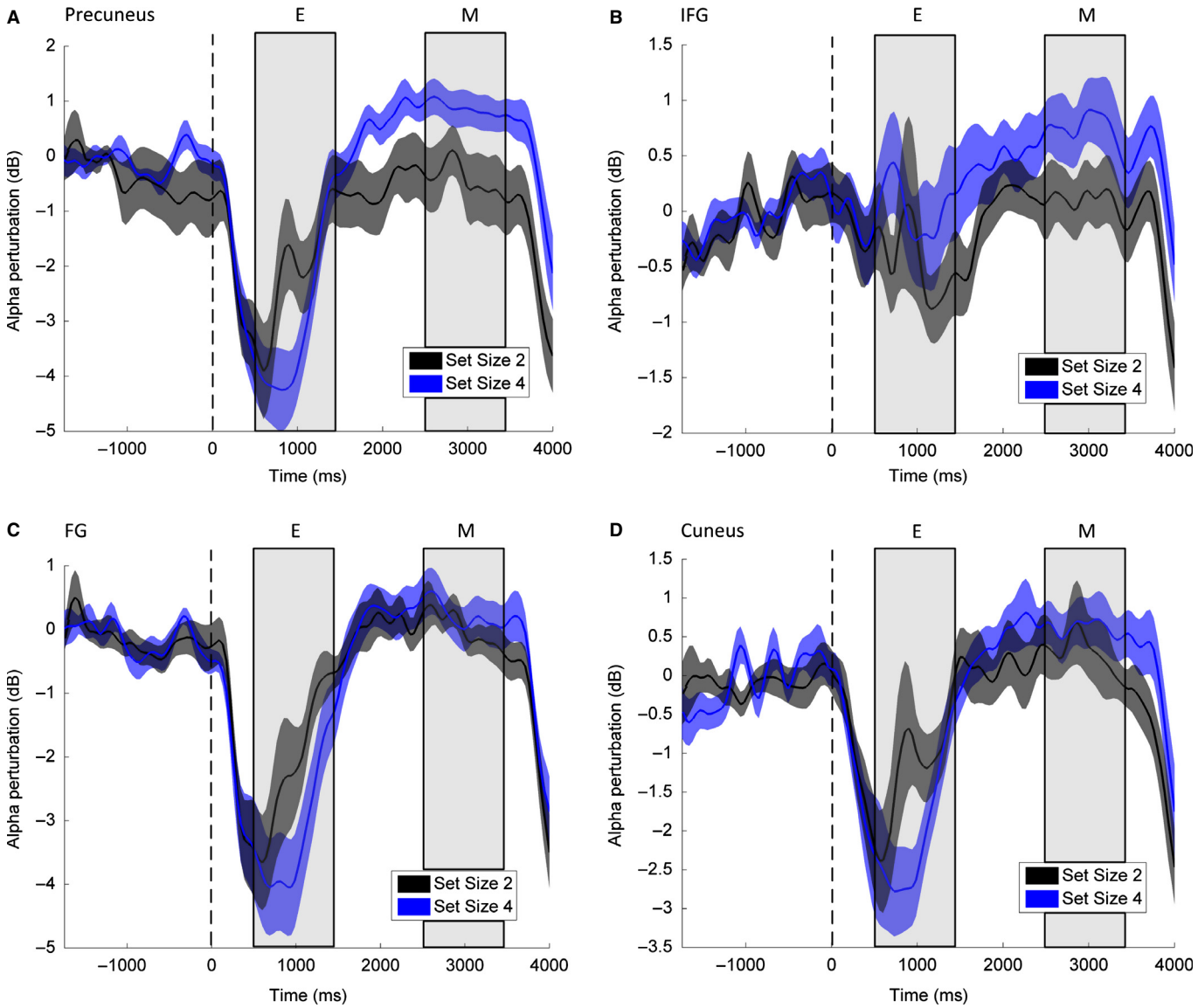

FIG. 6. Time-course of α-power of select components. (A) α-Power (8–13 Hz) in precuneus decreased rapidly after presentation of the stimulus but elevated higher than prestimulus level; (B) α-power in IFG increased following the presentation of stimulus; (C and D) α-power in FG and cuneus decreased rapidly following presentation of stimlus but, unlike precuneus activity, decayed back to the prestimulus level. Vertical boxes indicate encoding (E) and maintenance (M) stages. Shaded bands represent ± 1 SEM.

significant modulations with varying set size load were considered for correlation analysis. Correlational analyses were corrected for multiple comparisons using FDR correction at the $\alpha = 0.05$ significance level (Benjamini & Yekutieli, 2001). For each neural metric (i.e. α-AEPC, α-AMPC and β-AEPC), correlation analysis was performed only for those ICs which showed reliable modulations across set sizes based on the initial ANOVA tests (α-AEPC: cuneus, precuneus, IPL and FG; β-AEPC: precuneus; α-AMPC: precuneus and IFG).

We examined whether individual WM capacity (calculated as the maximum WM capacity across set sizes) was related to differences in neural activity across various loads, as suggested by previous ERP (i.e., evoked response) studies (Vogel & Machizawa, 2004; Lefebvre *et al.*, 2013). However, we found no significant correlation between spectral brain measures and behavior. In comparison, the number of items stored in WM (i.e., K calculated for each set size and individual) was correlated with α- and β-AEPC in precuneus (α-AEPC: $r = -0.38$, $P = 0.02$; β-AEPC: $r = -0.30$, $P = 0.03$) and α-AMPC in the IFG ($r = 0.44$, $P = 0.003$; Fig. 8A–C), such that larger α-activity during WM encoding and maintenance predicted improved behavioral capacity. Correlations between response RT and accuracy with α/β power did not reach significance. Collectively, these findings indicate that individual WM capacity, as measured by K (but not response accuracy or RT, *per se*) is predicted by individual α/β neural oscillations during both memory encoding and maintenance stages.

Control experiments and analyses

Despite principal component analysis correction, induced brain responses are prone to ocular contamination, and residual eye movements may cause artifactual changes in the EEG spectrotemporal characteristics which masquerade as induced oscillatory responses (Yuval-Greenberg *et al.*, 2008). For example, it is possible that

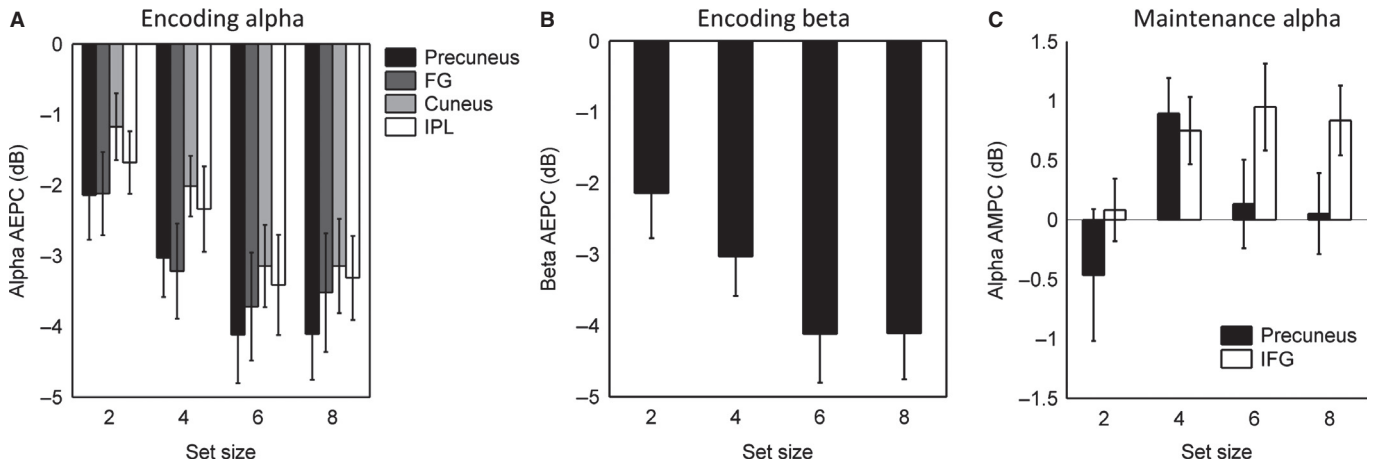

FIG. 7. Changes in EEG spectral characteristics with increasing memory load. (A) Encoding α-AEPC (8–13 Hz) increased linearly in occipital (cuneus), posterior parietal (precuneus and IPL) and temporal (FG) areas with increasing set size from 2 to 6 and plateaued thereafter. (B) β-AEPC (13–30 Hz) in precuneus increased with increasing set size from 2 to 6 and leveled out after set size 6. (C) α-AMPC (8–13 Hz) in precuneus, CG and IFG similarly increased with increasing memory load.

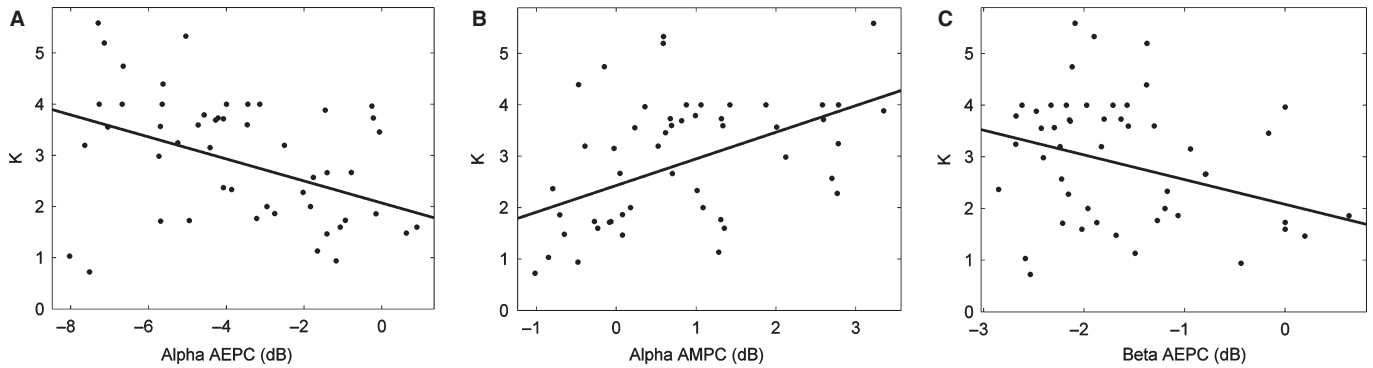

FIG. 8. Brain–behavioral correlations underlying visual WM capacity (K). Scatter plots show correlations between number of items stored in the memory and (A) α-AEPC (8–13 Hz) extracted from precuneus ($r = -0.38$, $P = 0.02$), (B) α-AMPC (8–13 Hz) in IFG ($r = 0.44$, $P = 0.003$) and (C) β-AEPC (13–30 Hz) extracted from precuneus ($r = -0.30$, $P = 0.03$). Behavioral WM performance was negatively and positively correlated with spectral power during encoding and maintenance respectively, suggesting individual visual WM capacity can be predicted based on oscillatory activity of the EEG. Each point corresponds to values extracted for a subject and set size (13 subjects and four set sizes).

subjects increase eye movement with increasing memory load; such artifacts would then co-vary with measured oscillatory α/β responses and would confound interpretation of our data. However, contamination of electrooculogram (EOG) activity on EEG recordings are most prevalent in prefrontal scalp locations and within lower frequency bands (i.e., delta and theta bands) (Hagemann & Naumann, 2001); EOG power is negligible at higher frequencies of the EEG where we observe our WM effects (i.e., α- and β-bands; Gasser *et al.*, 1985, 1986). Furthermore, it has been shown that artifact correction based on principal component analysis, which was employed in this study, reduces any residual artifact within these bands even further (with average error of < 0.1 dB; Wallstrom *et al.*, 2004). Collectively, the more posterior sources and higher-frequency modulations we report here make ocular contamination an unlikely cause of the observed effects.

Nonetheless, we aimed to quantitatively rule out the possibility that ocular movements may explain our data. To this end, we measured the frequency of subjects' blinks within the predefined 1-s encoding and maintenance periods where prominent WM modulations were observed in the EEG. For encoding, an ANOVA conducted on blink frequency showed a significant difference across conditions ($F_{3,42} = 35.94$, $P < 0.0001$). This was driven by a higher number of blinks in response to set size 2 than the other conditions (with a mean count of ~ 25 for set size 2 compared to ~ 0.5 for other set sizes). Consequently, we further compared α and β power for set size 2 responses by dividing the epochs into two data subsets: trials that did and did not contain blinks (i.e., contaminated vs uncontaminated epochs). A paired-samples *t*-test showed no difference in α or β power between the two data surrogates for either frequency band (α-AEPC: precuneus, $P = 0.46$; FG, $P = 0.44$; cuneus, $P = 0.44$; IPL, $P = 0.87$; β-AEPC: precuneus, $P = 0.36$), ruling out ocular contamination as a confounding factor. Similarly, for the maintenance period, blink frequency was invariant across conditions ($F_{3,42} = 1.51$, $P = 0.23$). Together, these observations suggest that modulations in α and β activity are unlikely to reflect residual ocular artifacts but, rather, reflect induced brain activity due to WM processing.

It is also important to note that an increased number of characters in the SET array may have led to the increase in α and β-AEPC during stimulus presentation. In addition, the α activity before presentation of the test character (TEST) might be linked to the effect of α on correct vs incorrect detection (Van Dijk *et al.*, 2008). In

order to investigate this possibility, an additional control experiment ($n = 4$) was conducted in which we examined the changes in brain response with a constant set size (load = 1) and changing stimulus size (i.e. 2, 4, 6, 8 copies of the same character). This control condition holds memory load constant but allows us to assess variation in brain activity with increasing stimulus complexity. No significant differences in the ROIs across set sizes were observed in α-AEPC (precuneus, $P = 0.25$; FG, $P = 0.45$; cuneus, $P = 0.34$; IPL, $P = 0.44$), α-AMPC (precuneus, $P = 0.1$; IFG, $P = 0.27$) or β-AEPC ($P = 0.76$; data not shown). Thus, it is unlikely that modulations in the observed brain areas are determined by stimulus properties alone. Rather, these results support the notion that the observed neural oscillatory activity is directly related to WM processing.

Discussion

We examined oscillatory brain responses during a Sternberg visual WM task with simultaneous presentation of a memory array. In simultaneous presentation, by changing the number of characters presented within a fixed time (500 ms) we varied the rate of information throughput of the corresponding brain pathways subserving WM processing. During visual stimulus encoding, α-band power parametrically decreased with memory load in occipital, parietal and temporal areas with a linear pattern that plateaued on set size 8 (above behavioral K capacity). Conversely, a load-dependent enhancement was observed in the same frequency band during the maintenance period in parietal and frontal areas which leveled out after set size 4 (around K). The distinct spectral characteristics of the brain activity during encoding and maintenance periods implies the existence of two separate networks engaged during each stage. Furthermore, it was shown that individual WM capacity (K) is related to spectral characteristics of EEG (α and β oscillations) within both encoding and maintenance stages.

Our findings are largely congruent with previous EEG and MEG studies which found a similar increase in α-power in posterior, central and frontal areas during WM maintenance (Krause *et al.*, 1996; Jensen *et al.*, 2002). Based on these observations, we propose that the precuneus area acts as a buffer with connections to both occipital and frontal areas for hypothetically encoding and active maintenance of visual information.

Psychophysiological explanations of encoding and active maintenance activity

In precuneus, the distinct spectral characteristics of the two-stage activity were suggestive of two distinct functions within the same brain region. This was evident by the load dependent decrease and increase in α-power during the encoding and maintenance stages. We posit that these two different events may correspond to the two processing periods of our task, describing the differential activation of encoding and maintenance of information in WM. The decreasing and increasing α-power trends during encoding and maintenance stages are generally in line with the gating by inhibition hypothesis (Jensen & Mazaheri, 2010), which suggests that information pathways within brain networks are controlled by task-dependent gating mechanisms. It is hypothesised that α- and γ-band oscillations play a pivotal role in this model. Active processing is reflected through γ-band synchronisation accompanied by α-band desynchronisation. Conversely, inhibition of task-irrelevant regions is reflected through elevated activity in the α-band, consistent with its putative role in attentional suppression (Foxe & Snyder, 2011) and/or network coordination and communication (Palva & Palva, 2007). Essentially, the increased α activity we observed in precuneus could be interpreted as isolation of WM by blocking the encoding pathway and preserving its current content in the memory store.

Moreover, results presented here further suggest that these oscillatory activities, namely in the α-band, may shift into different modes (excitation or inhibition) during the time-course of a cognitive operation. The abrupt α-power increase in IFG between low and high loads would imply that IFG is suppressed (and/or abruptly stressed) during higher processing demands. Nevertheless, another possible explanation could be due to executive functions reflecting 'top-down' processing such as mental rehearsal and corticocortical interactions (Von Stein & Sarnthein, 2000). This also suggests that, for lower load, rehearsal remains inactive and it becomes active during higher memory loads through an interaction between IFG and precuneus (see Fig. 7C). While covariation in the functional responses between these two regions suggests possible interaction, further causality analysis would be needed to confirm the validity of this hypothesis.

Spatial distribution of encoding and maintenance pathways

Dipole localisation results obtained in the current study are also generally consistent with findings from previous neuroimaging work examining verbal working memory. Specifically, Cohen *et al.* (1997) illustrated significant changes in BOLD signal in central occipital areas (BA17), Broca's area (BA44) and right DLPFC (BA9) during an n-back memory task. They further hypothesised that brain areas associated with active maintenance would demonstrate sustained activation throughout the trial, whereas those representing other WM processes would show transient activation but would grow with increasing load level. Sustained responses were observed in frontal (BA46/9/40) and parietal (BA40) areas, and time-dependent activities in visual (BA17) and parietal (BA40) areas. Corroborating activation was observed in the visual area (BA17) in which transient responses were recorded during WM maintenance. On the other hand, activity in right DLPFC showed a step-like function with load similar to the IFG activation found in the current study. Interestingly, load modulated transient activity was also reported in regions directly adjacent to those with sustained behavior in posterior parietal cortex (BA40). This suggests the co-occurrence of encoding and maintenance activity in the same region. Kirschen *et al.* (2010) also found similar activation in left frontal (BA6/9/44), bilateral inferior parietal (BA40) and occipital (BA19) cortices using a Sternberg task. In congruence with these findings, our results reveal: (i) a transient response which existed dominantly in sensory visual areas (cuneus) and FG; (ii) continuous activity in frontal areas (IFG) which increased abruptly from low (set size 2) to high (set sizes 4, 6, and 8; Fig. 7C) load; and (iii) dual stage activity in parietal areas (precuneus) marked by negative and positive changes in α activity during memory encoding and maintenance, respectively.

The relative locations of dipoles found in precuneus, FG, IPL and cuneus, which all shared the initial decrease in α-power, suggest a network extending from the visual cortices to parietal (precuneus) and temporal (FG) cortices, akin to the well-known ventral and dorsal visual streams (i.e., the 'what/where' pathway) responsible for processing visual object identification (recognition) and spatial location (Ungerleider *et al.*, 1998). The dorsal pathway may in turn activate frontal brain areas, as suggested by the common abrupt increase in α-power (e.g., precuneus and IFG). Conceivably, such frontal brain mechanisms may act to gate or update the WM 'buffer'. Together, this network may form and/or integrate with aspects

of the so-called phonological loop described in neurocognitive models of WM (Baddeley, 2000). Correspondingly, a recent meta-analysis study of working memory fMRI experiments unveiled that the most consistent areas experiencing WM load effects were associated with bilateral networks distributed on frontal and parietal areas and specifically the inferior frontal gyri (Rottschy *et al.*, 2012), which is quite consistent with the frontal activity observed in this study (IC2 in IFG). Additionally, engagement of this area during verbal tasks, which is confirmed in almost all previous studies comparing verbal and non-verbal memory tasks (Rottschy *et al.*, 2012), could reflect verbal rehearsal as part of the phonological loop of Baddeley's WM model.

Spectrotemporal activity during encoding predicts individual WM capacity

The drop in behavioral accuracy and saturation in RT, as well as the individual WM capacity (*K*) trends, all indicated that the WM capacity of our subject cohort was ~ 4 items. Hence, if α-power truly reflects the active representations of items maintained in WM, we would have expected no difference in power for set sizes above the capacity limit (~ 4). In congruence with behavioral results, α-AMPC in precuneus and IFG indeed saturated for set sizes > 4 and the maintenance activity in these areas was found to be highly correlated with *K* (see Fig. 8B).

Findings from previous ERP studies have suggested a relationship between WM capacity and neural activity during the WM maintenance period (Vogel & Machizawa, 2004; Grimault *et al.*, 2014). Our observations corroborate and extend these results by implicating a possible relationship between encoding activity and individual WM capacity (Fig. 8A and C). Significant correlations found between *K* values and encoding stage activity suggests that neurophysiological responses during stimulus information encoding may play a key role in an individual's success in later recall and WM performance. Specifically, the significant correlation found between *K* and α- and β-power in precuneus suggests that, in individuals with lower WM capacity, encoding activity grows less when they are exposed to higher loads. This finding may also be related to recent findings by Lenartowicz *et al.* (2014) in a study on attention-deficit/hyperactivity disorder (ADHD) patients. They reported attenuated α-band desynchronisation during the encoding period in ADHD patients and suggested that performance deficits in ADHD patients may have been the consequence of poor vigilance and atypical encoding. In addition, they found strong correlations between several behavioral responses including accuracy and response time with encoding α desynchronisation. Nonetheless, while several other studies have reported significant changes in spectral characteristics of EEG in response to changing memory load (Jensen *et al.*, 2002; Schack & Klimesch, 2002; Tuladhar *et al.*, 2007; Okuhata *et al.*, 2013), to the best of our knowledge no previous work has reported correlations between individual WM capacity and spectral characteristics of the EEG. Our findings provide a novel insight into WM by revealing the significance of neuronal spectrotemporal features (α and β oscillations) in predicting WM capacity and highlight the importance of brain processing during stimulus encoding in dictating success in WM tasks.

Conclusion

Spectrotemporal dynamics of brain responses revealed negative and positive power changes, primarily within α-band, in frontal and parietal cortices during encoding and maintenance stages. Possible contributions from other overlapping neural processes were reduced through application of ICA. In line with the hypothesis of the activation and inhibition role of α-activity in brain networks, we found a systematic decrease in α-power during memory encoding followed by an increase during WM maintenance. Correlation analysis showed that α- and β-band oscillations evoked during stimulus encoding and maintenance were strongly correlated with individual WM capacity as measured behaviorally. These results contribute to the general understanding of brain mechanisms related to working memory and suggest that neural oscillatory activity of the EEG changes its functional role over the time-course of a cognitive operation.

Conflict of interest

The authors declare no competing financial interests.

Acknowledgements

This work was partially supported by the Electrical and Computer Engineering Department and NSF grant NSF-IIS-0746790. Any opinions, findings, and conclusions or recommendations expressed in this material are those of the authors and do not necessarily reflect the views of the funding institution.

Abbreviations

AEPC, average encoding power change; AMPC, average maintenance power change; BOLD, blood oxygen level-dependent; EEG, electroencephalography; ERP, event-related potential; ERSP, event related spectral perturbation; FDR, false discovery rate; FG, fusiform gyrus; fMRI, functional magnetic resonance imaging; IC, independent component; ICA, independent component analysis; IFG, inferior frontal gyrus; IPL, inferior parietal lobule; *K*, WM capacity index; MEG, magnetoencephalography; rm, repeated-measures (ANOVA); RT, response time; RV, residual variance; WM, working memory.

References

Baddeley, A. (2000) The episodic buffer: a new component of working memory? *Trends Cogn. Sci.*, **4**, 417–423.
Benjamini, Y. & Yekutieli, D. (2001) The control of the false discovery rate in multiple testing under dependency. *Ann. Stat.*, **29**, 1165–1188.
Bidelman, G.M., Moreno, S. & Alain, C. (2013) Tracing the emergence of categorical speech perception in the human auditory system. *NeuroImage*, **79**, 201–212.
Bidelman, G.M., Villafuerte, J.W., Moreno, S. & Alain, C. (2014) Age-related changes in the subcortical-cortical encoding and categorical perception of speech. *Neurobiol. Aging*, **35**, 2526–2540.
Brainard, D.H. (1997) The psychophysics toolbox. *Spatial Vision*, **10**, 433–436.
Cohen, J.D., Perlstein, W.M., Braver, T.S., Nystrom, L.E., Nolls, D.C., Jonides, J. & Smith, E.E. (1997) Temporal dynamics of brain activation during a working memory task. *Nature*, **386**, 604–608.
Cowan, N. (2000) The magical number 4 in short-term memory: a reconsideration of mental storage capacity. *Behav. Brain Sci.*, **24**, 87–185.
Cowan, N. (2005) *Working Memory Capacity*. Psychology Press, New York, NY, USA.
Delorme, A. & Makeig, S. (2004) EEGLAB: an open source toolbox for analysis of single-trial EEG dynamics including independent component analysis. *J. Neurosci. Meth.*, **134**, 9–21.
Foxe, J.J. & Snyder, A.C. (2011) The role of alpha-band brain oscillations as a sensory suppression mechanism during selective attention. *Front .Psychol.*, **2**, 154.
Gasser, T., Sroka, L. & Möcks, J. (1985) The transfer of EOG activity into the EEG for eyes open and closed. *Electroen. Clin. Neuro.*, **61**, 181–193.
Gasser, T., Sroka, L. & Möcks, J. (1986) The correction of EOG artifacts by frequency dependent and frequency independent methods. *Psychophysiology*, **23**, 704–712.
Golob, E.J. & Starr, A. (2004) Serial position effects in auditory event-related potentials during working memory retrieval. *J. Cognitive Neurosci.*, **16**, 40–52.

Grimault, S., Nolden, S., Lefebvre, C., Vachon, F., Hyde, K., Peretz, I., Zatorre, R., Robitaille, N. & Jolicoeur, P. (2014) Brain activity is related to individual differences in the number of items stored in auditory short-term memory for pitch: evidence from magnetoencephalography. *NeuroImage*, **94**, 96–106.

Hagemann, D. & Naumann, E. (2001) The effects of ocular artifacts on (lateralized) broadband power in the EEG. *Clin. Neurophysiol.*, **112**, 215–231.

Herrmann, C.S., Mecklinger, A. & Pfeifer, E. (1999) Gamma responses and ERPs in a visual classification task. *Clin. Neurophysiol.*, **110**, 636–642.

Jensen, O. & Mazaheri, A. (2010) Shaping functional architecture by oscillatory alpha activity: gating by inhibition. *Front. Hum. Neurosci.*, **4**, 186.

Jensen, O., Gelfand, J., Kounios, J. & Lisman, J.E. (2002) Oscillations in the alpha band (9-12 Hz) increase with memory load during retention in a short-term memory task. *Cereb. Cortex*, **12**, 877–882.

Jung, T.P., Makeig, S., Westerfield, M., Townsend, J., Courchesne, E. & Sejnowski, T.J. (2001) Analysis and visualization of single-trial event-related potentials. *Hum. Brain Mapp.*, **14**, 166–185.

Kirschen, M.P., Chen, S.H.A. & Desmond, J.E. (2010) Modality specific cerebro-cerebellar activations in verbal working memory: an fMRI study. *Behav. Neurol.*, **23**, 51–63.

Krause, C.M., Lang, A.H., Laine, M., Kuusisto, M. & Pörn, B. (1996) Event-related EEG desynchronization and synchronization during an auditory memory task. *Electroen. Clin. Neuro.*, **98**, 319–326.

Lee, T.W., Girolami, M. & Sejnowski, T.J. (1999) Independent component analysis using an extended infomax algorithm for mixed subgaussian and supergaussian sources. *Neural Comput.*, **11**, 417–441.

Lefebvre, C., Vachon, F., Grimault, S., Thibault, J., Guimond, S., Peretz, I., Zatorre, R.J. & Jolicœur, P. (2013) Distinct electrophysiological indices of maintenance in auditory and visual short-term memory. *Neuropsychologia*, **51**, 2939–2952.

Lenartowicz, A., Delorme, A., Walshaw, P.D., Cho, A.L., Bilder, R.M., McGough, J.J., McCracken, J.T., Makeig, S. & Loo, S.K. (2014) Electroencephalography correlates of spatial working memory deficits in attention-deficit/hyperactivity disorder: vigilance, encoding, and maintenance. *J. Neurosci.*, **34**, 1171–1182.

Luck, S.J. & Vogel, E.K. (1997) The capacity of visual working memory for features and conjunctions. *Nature*, **390**, 279–281.

Makeig, S. (1993) Auditory event-related dynamics of the EEG spectrum and effects of exposure to tones. *Electroen. Clin. Neuro.*, **86**, 283–293.

Makeig, S., Bell, A.J., Jung, T.-P. & Sejnowski, T.J. (1996) Independent component analysis of electroencephalographic data. *Adv. Neur. In.*, **8**, 145–151.

Makeig, S., Debener, S., Onton, J. & Delorme, A. (2004) Mining event-related brain dynamics. *Trends Cogn. Sci.*, **8**, 204–210.

Meltzer, J.A., Negishi, M., Mayes, L.C. & Constable, R.T. (2007) Individual differences in EEG theta and alpha dynamics during working memory correlate with fMRI responses across subjects. *Clin. Neurophysiol.*, **118**, 2419–2436.

Meltzer, J.A., Zaveri, H.P., Goncharova, II, Distasio, M.M., Papademetris, X., Spencer, S.S., Spencer, D.D. & Constable, R.T. (2008) Effects of working memory load on oscillatory power in human intracranial EEG. *Cereb. Cortex*, **18**, 1843–1855.

Okuhata, S., Kusanagi, T. & Kobayashi, T. (2013) Parietal EEG alpha suppression time of memory retrieval reflects memory load while the alpha power of memory maintenance is a composite of the visual process according to simultaneous and successive Sternberg memory tasks. *Neurosci. Lett.*, **555**, 79–84.

Oldfield, R.C. (1971) The assessment and analysis of handedness: the Edinburgh inventory. *Neuropsychologia*, **9**, 97–113.

Oostendorp, T.F. & Van Oosterom, A. (1989) Source parameter estimation in inhomogeneous volume conductors of arbitrary shape. *IEEE T. Bio.-med. Eng.*, **36**, 382–391.

Oostenveld, R. & Praamstra, P. (2001) The five percent electrode system for high-resolution EEG and ERP measurements. *Clin. Neurophysiol.*, **112**, 713–719.

Palva, S. & Palva, J.M. (2007) New vistas for alpha-frequency band oscillations. *Trends Neurosci.*, **30**, 150–158.

Pashler, H. (1988) Familiarity and visual change detection. *Percept. Psychophys.*, **44**, 369–378.

Pfurtscheller, G. & Lopes, F.H. (1999) Event-related EEG/MEG synchronization and desynchronization : basic principles. *Clin. Neurophysiol.*, **110**, 1842–1857.

Rottschy, C., Langner, R., Dogan, I., Reetz, K., Laird, A.R., Schulz, J.B., Fox, P.T. & Eickhoff, S.B. (2012) Modelling neural correlates of working memory: a coordinate-based meta-analysis. *NeuroImage*, **60**, 830–846.

Salo, E., Rinne, T., Salonen, O. & Alho, K. (2013) Brain activity during auditory and visual phonological, spatial and simple discrimination tasks. *Brain Res.*, **1496**, 55–69.

Schack, B. & Klimesch, W. (2002) Frequency characteristics of evoked and oscillatory electroencephalic activity in a human memory scanning task. *Neurosci. Lett.*, **331**, 107–110.

Schomer, D.L. & Da Silva, F.L. (2012) *Niedermeyer's Electroencephalography: basic Principles, Clinical Applications, and Related Fields*. Wolters Kluwer Health, Philadelphia, PA, USA.

Sternberg, S. (1966) High-speed scanning in human memory. *Science*, **153**, 652–654.

Tallon-Baudry, C., Bertrand, O., Wienbruch, C., Ross, B. & Pantev, C. (1997) Combined EEG and MEG recordings of visual 40 Hz responses to illusory triangles in human. *NeuroReport*, **8**, 1103–1107.

Tang, A.C., Pearlmutter, B.A., Malaszenko, N.A., Phung, D.B. & Reeb, B.C. (2002) Independent components of magnetoencephalography: localization. *Neural Comput.*, **14**, 1827–1858.

Todd, J.J. & Marois, R. (2004) Capacity limit of visual short-term memory in human posterior parietal cortex. *Nature*, **428**, 751–754.

Tuladhar, A.M., ter Huurne, N., Schoffelen, J.-M., Maris, E., Oostenveld, R. & Jensen, O. (2007) Parieto-occipital sources account for the increase in alpha activity with working memory load. *Hum. Brain Mapp.*, **28**, 785–792.

Ungerleider, L.G., Courtney, S.M. & Haxby, J.V. (1998) A neural system for human visual working memory. *Proc. Natl. Acad. Sci. USA*, **95**, 883–890.

Vakorin, V.A., Kovacevic, N. & McIntosh, A.R. (2010) Exploring transient transfer entropy based on a group-wise ICA decomposition of EEG data. *NeuroImage*, **49**, 1593–1600.

Van Dijk, H., Schoffelen, J.-M., Oostenveld, R. & Jensen, O. (2008) Prestimulus oscillatory activity in the alpha band predicts visual discrimination ability. *J. Neurosci.*, **28**, 1816–1823.

Vigário, R., Särelä, J., Jousmäki, V., Hämäläinen, M. & Oja, E. (2000) Independent component approach to the analysis of EEG and MEG recordings. *IEEE T. Bio.-med. Eng.*, **47**, 589–593.

Vogel, E.K. & Machizawa, M.G. (2004) Neural activity predicts individual differences in visual working memory capacity. *Nature*, **428**, 748–751.

Von Stein, A. & Sarnthein, J. (2000) Different frequencies for different scales of cortical integration: from local gamma to long range alpha/theta synchronization. *Int. J. Psychophysiol.*, **38**, 301–313.

Wallstrom, G.L., Kass, R.E., Miller, A., Cohn, J.F. & Fox, N.A. (2004) Automatic correction of ocular artifacts in the EEG: a comparison of regression-based and component-based methods. *Int. J. Psychophysiol.*, **53**, 105–119.

Yuval-Greenberg, S., Tomer, O., Keren, A.S., Nelken, I. & Deouell, L.Y. (2008) Transient induced gamma-band response in EEG as a manifestation of miniature saccades. *Neuron*, **58**, 429–441.

Zoefel, B. & Heil, P. (2013) Detection of near-threshold sounds is independent of EEG phase in common frequency bands. *Front. Psychol.*, **4**, 262.